



Synthesis and application of a novel nanomagnetic catalyst with Cl[DABCO-NO₂]C(NO₂)₃ tags in the preparation of pyrazolo[3,4-*b*]pyridines via anomeric based oxidation

Javad Afsar¹ · Mohammad Ali Zolfigol¹ · Ardeshir Khazaei¹ · Diego A. Alonso² · Abbas Khoshnood² · Yadollah Bayat³ · Asiye Asgari³

Received: 11 June 2018 / Accepted: 25 August 2018 / Published online: 5 September 2018
© Springer Nature B.V. 2018

Abstract

A novel nanomagnetic catalyst with Cl[DABCO-NO₂]C(NO₂)₃ tags was designed, synthesized and fully characterized by several techniques such as Fourier transform infrared spectroscopy, energy-dispersive X-ray spectroscopy, elemental mapping analysis, thermogravimetric analysis, derivative thermal gravimetric, powder X-ray diffraction patterns, field scanning electron microscopy, high resolution transmission electron microscopy, physical adsorption and desorption of N₂ isotherms (BET) and vibrating sample magnetometer. The synthesized nanomagnetic particles were used as an efficient and recyclable catalyst for the one-pot three component condensation reaction of 3-methyl-1-phenyl-1*H*-pyrazol-5-amine or 3-methyl-1*H*-pyrazol-5-amine, aryl aldehydes and malononitrile for the synthesis of pyrazolo[3,4-*b*]pyridine derivatives under neat conditions.

Keywords Pyrazolo[3,4-*b*]pyridine · Nanomagnetic catalyst · Fe₂O₃@SiO₂(CH₂)₃-Cl[DABCO-NO₂]C(NO₂)₃ · Solvent-free · Anomeric-based oxidation

Electronic supplementary material The online version of this article (<https://doi.org/10.1007/s11164-018-3576-9>) contains supplementary material, which is available to authorized users.

✉ Mohammad Ali Zolfigol
zolfi@basu.ac.ir; mzolfigol@yahoo.com

Ardeshir Khazaei
Khazaei_1326@yahoo.com

Diego A. Alonso
diego.alonso@ua.es

Abbas Khoshnood
abbas.khoshnood@ua.es; abbaskhoshnood@yahoo.com

Extended author information available on the last page of the article

Introduction

The outlook of chemical processes is moving towards the goal of sustainable development. With this aim, the design, synthesis and applications of “benign” catalysts has been one of the serious challenges for chemists and chemical engineers in recent years. Nowadays, chemical processes that produce the least waste and pollutants are of paramount importance. One way to achieve this goal is to use catalysts that increase a chemical reaction’s rate by reducing its activation energy, simultaneously reducing energy consumption [1]. Homogeneous catalysts have demonstrated good performance in chemical processes, but their separation from the reaction mixture is tediously long, so the use of heterogeneous catalysts, especially highly efficient nano-catalysts, is highly interesting [2–6]. However, nano-sized catalysts are difficult to separate from the reaction mixture by conventional filtration techniques. Nanomagnetic catalysts are designed to solve this problem. Generally, these catalysts can be easily separated from the reaction by using a magnet and reused several times with only a marginal decrease in reactivity [7–13].

Multi-component reactions (MCRs) have been introduced and developed in order to increase the efficiency of chemical reactions, simplify processes, save time and energy, increase the atomic economy and reduce the use of organic solvents and waste generation [14–16].

The influence of the stereoelectronic anomeric effect on the reactivity of certain chemical entities has been extensively reviewed [17–20]. Recently, the term “anomeric based oxidation (ABO)” has been introduced to explain the driving force for the aromatization of susceptible heterocyclic compounds, those which have heteroatoms at the appropriate sites, by an exceptional hydride transfer mechanism. In addition to experimental observations, computational evidence also confirms this mechanism [21]. The systematic study of the anomeric effect in target molecules allows the design of synthetic strategies based on anomerically driven stereoselective reactions, or highly biased equilibrium between isomeric products. Many biological processes involve an oxidation–reduction step of substrates by NAD^+ / NADH and/or NADP^+ / NADPH , respectively (Fig. 1). The key feature of the oxidation mechanism in these systems is a hydride transferring from carbon to substrates via anomeric based oxidation. Thus, the development of anomeric based oxidation and/or aromatization reactions can be expected to lead to a knowledge-based design of biomimetic reactions in the future. We think that the obtained results from this field of research will support the idea of rational designs, syntheses and applications of tasked-specific catalysts and molecules for the development of anomeric based oxidation and/or aromatization mechanisms [22–25].

Pyrazole derivatives have attracted much interest due to their variety of biological and pharmacological activities such as antiviral [26], antidiabetic [27], hypotensive [28], anticancer [29], antitumor, antibacterial [30] and anti-inflammatory [31]. These compounds can be also effective in the remedy of gastrointestinal disease, drug and alcohol withdrawal symptoms, anorexia nervosa depression, hemorrhaged stress, Alzheimer’s disease, infertility and drug addiction [32, 33]. Recently, it has been found that pyrazolo[3,4-*b*]pyridines can also be used as FGFR Kinase inhibitors [34]

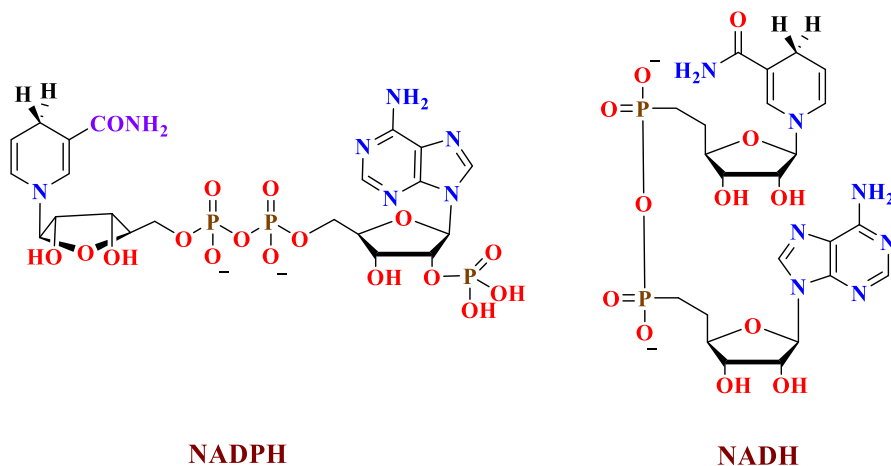


Fig. 1 Molecular structures of NADH and NADPH

and metabotropic glutamate receptor 5 (mGluR5) [35] (Fig. 2). Therefore, due to these important biological abilities, any development in the synthetic organic methodology for the preparation of these compounds is potentially important.

With this aim, we wish to introduce $\text{Fe}_2\text{O}_3@\text{SiO}_2(\text{CH}_2)_3\text{-Cl}[\text{DABCO-NO}_2]\text{-C}(\text{NO}_2)_3$ as a novel nanomagnetic catalyst and use it as an efficient and reusable catalyst in the synthesis of pyrazolo[3,4-*b*]pyridine derivatives via anomeric based oxidation under solvent-free conditions (Scheme 1).

Experimental

General

All chemicals were obtained from Merck or Sigma-Aldrich and were used without further purification. Known products were identified by comparison of their melting

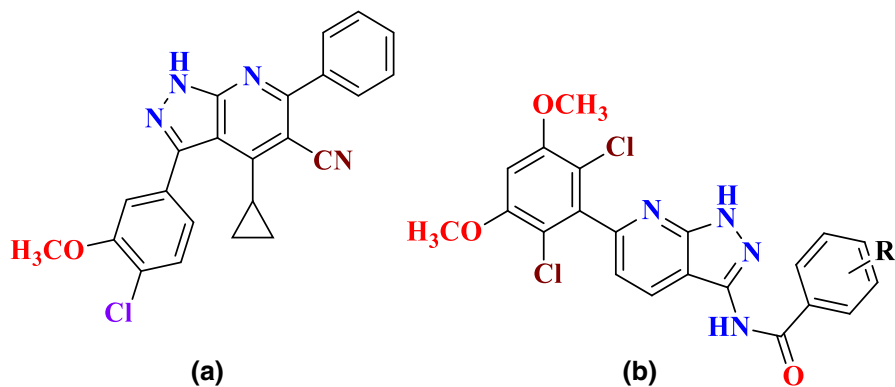
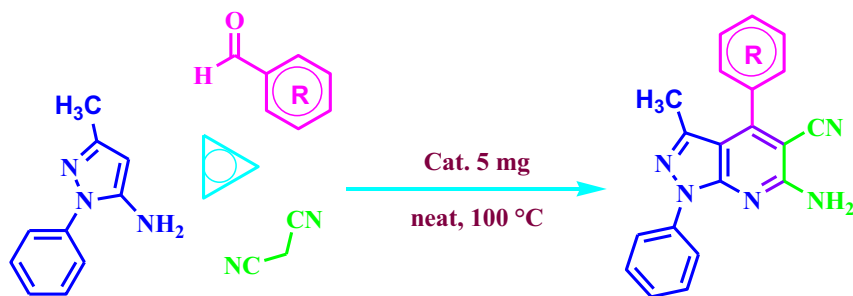


Fig. 2 **a** FGFR Kinase Inhibitors, **b** metabotropic glutamate receptor 5 (mGluR5)



R: H, 4-Cl, 4-Me, 4-MeO, 2,4-Cl₂, 4-Isopropyle, 4-Br, 4-NO₂, 3,4-(MeO)₂, 4-F, 3-NO₂, 2,6-F₂, 3,5-F₂, 3,4-F₂, 4-CN, 2-Naph, 1-Naph

Scheme 1 MCRs Synthesis of pyrazolo[3,4-*b*]pyridine derivatives using Fe₂O₃@SiO₂(CH₂)₃-Cl[DABCO-NO₂]C(NO₂)₃ as novel nanomagnetic catalyst under neat conditions

points and spectral data with those reported in the literature. Progress of the reactions was monitored by TLC using silica gel SIL G/UV 254 plates. Melting points were recorded on a Büchi B-545 apparatus in open capillary tubes. *R_f* values were measured using a 3/7 mixture of EtOAc/*n*-Hexane as eluent. Fourier transformed infrared (FTIR) spectra of the catalyst and the synthesized products were performed on a Perkin-Elmer spectrum 65 FT-IR spectrometer using KBr disks. High resolution mass spectra (GC/QTOF, chemical ionization (CI) mode with 20% CH₄ and 300 °C source temperature) were obtained using an Agilent 7200 Network spectrometer. Each sample was dissolved in CHCl₃ and directly injected into the instrument by using a standard Agilent glass capillary. ¹H NMR (300 and 400 MHz) spectra were obtained on Bruker Avance 300 and Bruker Avance 400 NMR spectrometers under proton coupled mode using CDCl₃ as solvent. ¹³C NMR (75, 101 and 126 MHz) spectra were acquired on Bruker Avance 300, Bruker Avance 400 NMR and Bruker Avance DRX 500 NMR spectrometers in the proton decoupled mode at 20 °C in CDCl₃ as solvent. Chemical shifts are given in δ (parts per million) and the coupling constants (*J*) in Hertz. ¹⁹F NMR (282 and 376 MHz) spectra were recorded on Bruker Avance 300 and Bruker Avance 400 NMR spectrometers, in proton coupled mode. Data for ¹H NMR spectra are reported as follows: chemical shift (ppm), multiplicity (s, singlet; d, doublet; t, triplet; q, quartet; m, multiplet; and br., broad), coupling constant (Hz), and integration. Simultaneous thermal gravimetry analysis TG-DSC, were carried out on a Mettler Toledo device (model TGA/SDTA851and/LF/1600), capable of working between room temperature and 1600 °C under inert Argon atmosphere and equipped with a 34 position autosampler. The experiment was carried out at 25 °C using a heating rate of 25 °C min⁻¹ up to 800 °C. The powder X-ray diffraction (XRD) pattern was recorded with a Bruker D8-Advance with a Goebel mirror (non-planar samples), high temperature chamber (up to 900 °C), generator of x-ray KRISTALLOFLEX K 760-80F (power: 3000 W, voltage: 20–60 kV and current: 5–80 mA) and with a tube of RX with copper anode Kα (λ = 0.154 nm) in the range 10° < 2θ < 90°.

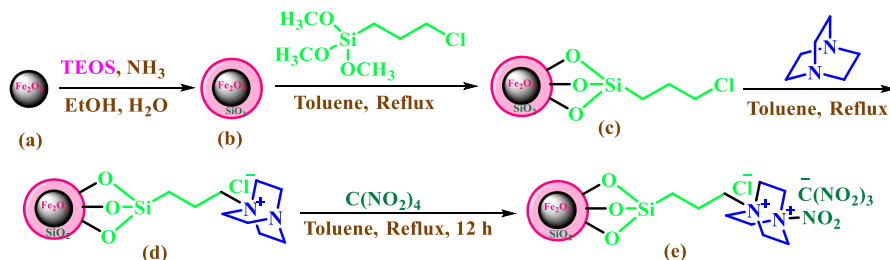
Physical adsorption and desorption of N_2 isotherms were measured at 77 K with an AUTOSORB-iQ-XR-2 analyzer. The catalyst was degassed before the experiment for 1 day at 100 °C under high vacuum conditions. The Brunauer–Emmett–Teller (BET) method was used to calculate the specific surface areas (S_{BET}). By using the Barrett–Joyner–Halenda (BJH) model, the pore volumes and pore size distributions were derived from the adsorption branches of isotherms. The micropore surface area (S_{BET} micro) was calculated using the $V-t$ plot method. Scanning electron microscopy (SEM) studies were performed using a Hitachi S3000N, equipped with a Bruker XFlash 3001 x-ray detector for microanalysis (EDX) and elemental mapping. Field emission scanning electron microscopy (FESEM) studies were performed using a Merlin VP Compact from Zeiss, equipped with a Bruker Quantax 400 EDS microanalysis system. The resolution was 0.8 nm at 15 kV and 1.6 nm at 1 kV. Field emission equipment is able to work at very reduced voltages (from 0.02 to 30 kV) allowing us to observe beam sensitive samples without damaging them and minimizing the charging effects. High-resolution transmission electron microscopy (HRTEM) images were obtained using a JEOL JEM-2010 microscope operating at an accelerating voltage of 200 kV. This microscope was equipped with an OXFORD INCA Energy TEM 100 x-ray detector for microanalysis (EDS) and acquisition of the images was made by means of a GATAN ORIUS SC600 digital camera mounted on-axis, integrated with the program GATAN Digital Micrograph 1.80.70 for GMS 1.8.0. The sample was prepared by drop casting the dispersed particles in absolute ethanol onto a 300-mesh copper grid from TED PELLA, INC. model 01883-F, coated with a lacey formvar film enforced by a heavy coating of carbon. Holes were completely open. The magnetic behavior of the nanomagnetic catalyst was also measured by a vibrating sample magnetometer (VSM) instrument from Meghnatis Daghig Kavir Company, model LBKFB.

General procedure for the preparation of the novel nanomagnetic catalyst

Fe_2O_3 nanoparticles were prepared according to a previously reported procedure. Then, 1 g of Fe_2O_3 nanoparticles (**a**) was dispersed in toluene. In the next step, to coat the surface of the Fe_2O_3 with SiO_2 , 1.5 mL tetraethyl orthosilicate (TEOS) was added drop-wise and the reaction was continued for 12 h under reflux conditions. The resultant $Fe_2O_3@SiO_2$ (**b**) was washed with ethanol for three times and dried. After that, in order to silanate the silica coated nanomagnetic particles, 3-chloropropyltrimethoxysilane (1.5 mL) was added to the mixture in toluene under reflux conditions to give (**c**). After 12 h, compound (**c**) was washed with ethanol, then 1,4-diazabicyclo[2.2.2]octane (DABCO) (6 mmol, 0.67 g) was added and refluxed in ethanol for 12 h to afford compound (**d**). Eventually, tetranitromethane (6 mmol, 1.18 g, 0.73 mL) was added to compound (**d**) in toluene under reflux conditions to give (**e**) as a novel nanomagnetic catalyst (Scheme 2).

General procedure for the synthesis of pyrazolo[3,4-*b*]pyridine derivatives

To a round-bottom flask containing a mixture of the corresponding aldehyde (1 mmol), 3-methyl-1-phenyl-1*H*-pyrazol-5-amine or 3-methyl-1*H*-pyrazol-5-



Scheme 2 Synthetic route for synthesis of novel nanomagnetic catalyst Fe₂O₃@SiO₂(CH₂)₃-Cl[DABCO-NO₂]C(NO₂)₃

amine (1 mmol) and malononitrile (1.2 mmol, 79 mg) 5 mg of Fe₂O₃@SiO₂(-CH₂)₃-Cl[DABCO-NO₂]C(NO₂)₃ were added. The resulting mixture was stirred magnetically under neat conditions at 100 °C. After completion of the reaction, which was monitored by TLC, the mixture was cooled to room temperature. Then, acetone was added to separate the catalyst by an external magnet. After evaporation of the solvent, the resulting solid was recrystallized in ethanol to give the corresponding pure products. Finally, the nanomagnetic catalyst was reused for the next run (Scheme 1).

Spectroscopic and analytical data for the synthesized products

6-Amino-3-methyl-1,4-diphenyl-1H-pyrazolo[3,4-*b*]pyridine-5-carbonitrile (1a) Isolated as white solid, (290 mg, 89%), R_f: 0.52; Melting point: 210–212 °C; FT-IR: ν (cm⁻¹) = 3366, 3219, 2217, 1626, 756; ¹H NMR (300 MHz) δ 8.11 (dd, *J* = 8.6, 1.1, 2H), 7.66–7.39 (m, 7H), 7.35–7.27 (m, 1H), 5.42 (br. s, 2H), 2.03 (s, 3H). ¹³C NMR (101 MHz) δ 158.3, 152.8, 150.9, 144.4, 138.8, 134.0, 129.9, 129.0, 128.6 (2c), 126.2, 121.5, 116.8, 109.5, 88.5, 14.7; HRMS calcd. for C₂₀H₁₅N₅ [M⁺] 325.1327, found: 325.1343.

6-Amino-4-(3,4-dimethoxyphenyl)-3-methyl-1-phenyl-1H-pyrazolo[3,4-*b*]pyridine-5-carbonitrile (1b) Isolated as white solid, (354 mg, 92%), R_f: 0.35; Melting point: 218–220 °C; FT-IR: ν (cm⁻¹) = 3332, 3222, 2210, 1626, 765; ¹H NMR (300 MHz) δ 8.10 (dd, *J* = 8.6, 1.1, 2H), 7.58–7.42 (m, 2H), 7.35–7.27 (m, 1H), 7.11–7.00 (m, 2H), 6.98 (d, *J* = 1.5, 1H), 5.41 (br. s, 2H), 3.98 (s, 3H), 3.94 (s, 3H), 2.13 (s, 3H). ¹³C NMR (101 MHz) δ 158.4, 152.7, 150.9, 150.3, 148.8, 144.4, 138.8, 129.0, 126.2 (2c), 121.7, 121.5, 117.1, 111.9, 111.0, 109.6, 88.6, 56.1, 56.0, 15.0; HRMS calcd. for C₂₂H₁₉N₅O₂ [M⁺] 385.1539, found: 385.1557.

6-Amino-3-methyl-4-(4-nitrophenyl)-1-phenyl-1H-pyrazolo[3,4-*b*]pyridine-5-carbonitrile (1c) Isolated as pale yellow solid, (333 mg, 90%), R_f: 0.60; Melting point: 223–225 °C; FT-IR: ν (cm⁻¹) = 3350, 3208, 2214, 1619, 1581, 1348, 769; ¹H NMR (300 MHz) δ 8.53–8.34 (m, 2H), 8.10 (d, *J* = 7.7, 2H), 7.79–7.59 (m, 2H), 7.51 (t, *J* = 7.9, 2), 7.33 (t, *J* = 7.4, 1H), 5.47 (br. s, 2H), 2.03 (s, 3H). ¹³C NMR (101 MHz) δ 158.1, 150.8, 149.7, 148.8, 143.6, 140.4, 138.5, 129.9, 129.0, 126.4, 124.0, 121.5,

116.1, 109.0, 88.0, 14.8; HRMS calcd. for $C_{20}H_{14}N_6O_2$ [M^+] 370.1178, found: 370.1187.

6-Amino-4-(4-chlorophenyl)-3-methyl-1-phenyl-1H-pyrazolo[3,4-*b*]pyridine-5-carbonitrile (1d) Isolated as white solid, (327 mg, 91%), R_f : 0.74; Melting point: 194–198 °C; FT-IR: ν (cm^{-1}) = 3308, 3187, 2214, 1633, 824; 1H NMR (300 MHz) δ 8.10 (dd, J = 8.5, 1.0, 2H), 7.61–7.45 (m, 4H), 7.45–7.38 (m, 2H), 7.31 (t, J = 7.4, 1H), 5.43 (br. s, 12H), 2.06 (s, 3H). ^{13}C NMR (101 MHz) δ 158.3, 151.3, 150.9, 144.1, 138.7, 136.3, 132.4, 130.0, 129.0 (2C), 126.3, 121.5, 116.6, 109.4, 88.4, 14.8; HRMS calcd. for $C_{20}H_{14}ClN_6$ [M^+] 359.0938, found: 370.0951.

6-Amino-4-(4-bromophenyl)-3-methyl-1-phenyl-1H-pyrazolo[3,4-*b*]pyridine-5-carbonitrile (1e) Isolated as white solid, (372 mg, 92%), R_f : 0.77; Melting point: 216–217 °C; FT-IR: ν (cm^{-1}) = 3369, 2920, 2217, 1637, 760; 1H NMR (300 MHz) δ 8.10 (dd, J = 8.6, 1.1, 2H), 7.75–7.67 (m, 2H), 7.54–7.45 (m, 2H), 7.38–7.28 (m, 3H), 5.43 (br. s, 2H), 2.06 (s, 3H). ^{13}C NMR (101 MHz) δ 158.3, 151.3, 150.9, 144.1, 138.7, 132.8, 132.0, 130.2, 129.0, 126.3, 124.5, 121.5, 116.6, 109.3, 88.3, 14.8; HRMS calcd. for $C_{20}H_{14}BrN_5$ [M^+] 403.0433, found: 403.0437.

6-Amino-4-(4-isopropylphenyl)-3-methyl-1-phenyl-1H-pyrazolo[3,4-*b*]pyridine-5-carbonitrile (1f) Isolated as white solid, (320 mg, 87%), R_f : 0.71; Melting point: 198–200 °C; FT-IR: ν (cm^{-1}) = 3308, 3190, 2211, 1635, 709; 1H NMR (300 MHz) δ 8.11 (dd, J = 8.6, 1.1, 12H), 7.53–7.45 (m, 2H), 7.40 (br. s, 4H), 7.34–7.27 (m, 1H), 5.42 (br. s, 2H), 3.10–2.93 (m, 1H), 2.06 (s, 3H), 1.34 (s, 3H), 1.32 (s, 3H). ^{13}C NMR (101 MHz) δ 158.4, 153.1, 150.9, 144.657, 138.8, 131.2, 129.0, 128.7, 126.6, 126.1, 121.5, 117.1, 109.6, 88.5, 34.0, 23.9, 14.8; HRMS calcd. for $C_{23}H_{21}N_5$ [M^+] 367.1797, found: 367.1812.

6-Amino-4-(2,4-dichlorophenyl)-3-methyl-1-phenyl-1H-pyrazolo[3,4-*b*]pyridine-5-carbonitrile (1g) Isolated as white solid, (359 mg, 91%), R_f : 0.82; Melting point: 167–169 °C; FT-IR: ν (cm^{-1}) = 3350, 3213, 2214, 1614, 757; 1H NMR (300 MHz) δ 8.11 (dd, J = 8.7, 1.1, 2H), 7.63 (d, J = 2.0, 1H), 7.55–7.42 (m, 3H), 7.35–7.27 (m, 2H), 5.45 (br. s, 2H), 2.02 (s, 3H). ^{13}C NMR (101 MHz) δ 158.2, 150.8, 148.2, 144.1, 138.7, 136.7, 133.5, 131.7, 130.8, 130.1, 129.0, 127.7, 126.3, 121.5, 115.9, 109.6, 88.8, 13.5; HRMS calcd. for $C_{20}H_{13}Cl_2N_5$ [M^+] 393.0548, found: 393.0564.

6-Amino-3-methyl-1-phenyl-4-(*p*-tolyl)-1H-pyrazolo[3,4-*b*]pyridine-5-carbonitrile (1h) Isolated as white solid, (315 mg, 93%), R_f : 0.72; Melting point: 200–202 °C; FT-IR: ν (cm^{-1}) = 3325, 3216, 2211, 1629, 762; 1H NMR (300 MHz) δ 8.16–8.07 (m, 2H), 7.54–7.44 (m, 2H), 7.36 (br. s, 4H), 7.33–7.27 (m, 1H), 5.39 (br. s, 2H), 2.47 (s, 3H), 2.07 (s, 3H). ^{13}C NMR (101 MHz) δ 158.4, 153.1, 150.9, 144.5, 140.0, 138.8, 131.0, 129.3, 129.0, 128.5, 126.2, 121.6, 117.0, 109.5, 88.5, 21.5, 14.8; HRMS calcd. for $C_{21}H_{17}N_5$ [M^+] 339.1484, found: 339.1495.

6-Amino-4-(4-fluorophenyl)-3-methyl-1-phenyl-1H-pyrazolo[3,4-*b*]pyridine-5-carbonitrile (1i) Isolated as white solid, (302 mg, 88%), R_f : 0.61; Melting point: 214–216 °C; FT-IR: ν (cm^{-1}) = 3328, 3222, 2214, 1629, 768; 1H NMR (300 MHz) δ 8.16–8.02 (m, 2H), 7.56–7.41 (m, 4H), 7.39–7.16 (m, 2H), 5.43 (br. s, 2H), 2.06

(s, 3H). ^{13}C NMR (101 MHz) δ 163.6 (d, $J = 250.4$), 158.3, 151.6, 150.9, 144.2, 138.7, 130.6 (d, $J = 8.5$), 129.9 (d, $J = 3.3$), 129.0, 126.3, 121.5, 116.7, 115.9 (d, $J = 22.0$), 109.5, 88.5, 14.8. ^{19}F NMR (282 MHz) δ -110.51 ; HRMS calcd. for $\text{C}_{20}\text{H}_{14}\text{FN}_5$ [M^+] 343.1233, found: 343.1244.

6-Amino-3-methyl-4-(3-nitrophenyl)-1-phenyl-1H-pyrazolo[3,4-*b*]pyridine-5-carbonitrile (1j) Isolated as white solid, (315 mg, 85%), R_f : 0.52; Melting point: 157–159 °C; FT-IR: ν (cm^{-1}) = 3357, 3224, 2216, 1617, 753; ^1H NMR (400 MHz) δ 8.46 (m, 1H), 8.38 (t, $J = 1.8$, 1H), 8.19–8.02 (m, 2H), 7.89–7.77 (m, 2H), 7.58–7.46 (m, 2H), 7.34 (m, 1H), 5.55 (br. s, 2H), 2.04 (s, 3H). ^{13}C NMR (75 MHz) δ 158.2, 149.4, 148.1, 143.6, 138.5, 138.1, 135.6, 134.5, 130.0, 129.0, 126.5, 124.8, 123.9, 122.8, 121.6, 116.2, 88.2, 14.8; HRMS calcd. for $\text{C}_{20}\text{H}_{14}\text{N}_6\text{O}_2$ [M^+] 370.1178, found: 393.1195.

6-Amino-4-(4-methoxyphenyl)-3-methyl-1-phenyl-1H-pyrazolo[3,4-*b*]pyridine-5-carbonitrile (1k) Isolated as white solid, (323 mg, 91%), R_f : 0.47; Melting point: 195–197 °C; FT-IR: ν (cm^{-1}) = 3353, 3224, 2216, 1629, 765; ^1H NMR (400 MHz) δ 8.17–8.04 (m, 2H), 7.52–7.46 (m, 2H), 7.44–7.39 (m, 2H), 7.33–7.27 (m, 1H), 7.09–7.05 (m, 2H), 5.40 (br. s, 2H), 3.90 (s, 3H), 2.10 (s, 3H). ^{13}C NMR (101 MHz) δ 160.9, 158.4, 152.8, 151.0, 144.5, 138.8, 130.2, 129.0, 126.1 (2C), 121.5, 117.2, 114.0, 109.7, 88.5, 55.4, 15.0.

6-Amino-4-(2,6-difluorophenyl)-3-methyl-1-phenyl-1H-pyrazolo[3,4-*b*]pyridine-5-carbonitrile (1l) Isolated as white solid, (307 mg, 85%), R_f : 0.55; Melting point: 227–229 °C; FT-IR: ν (cm^{-1}) = 3318, 3202, 2213, 1630, 768; ^1H NMR (300 MHz) δ 8.17–8.04 (m, 2H), 7.62–7.45 (m, 3H), 7.36–7.27 (m, 1H), 7.19–7.10 (m, 2H), 5.43 (br. s, 2H), 2.11 (s, 3H). ^{13}C NMR (101 MHz) δ 159.54 (dd, $J = 252.0$, 6.0), 158.2, 150.9, 143.9, 139.7, 138.6, 132.4 (t, $J = 10.0$), 129.0, 126.3, 121.6, 116.0, 112.0 (dd, $J = 19.5$, 6.0), 111.3 (t, $J = 20.0$), 110.0, 89.9, 13.0. ^{19}F NMR (282 MHz) δ -111.00 ; HRMS calcd. for $\text{C}_{20}\text{H}_{13}\text{F}_2\text{N}_5$ [M^+] 361.1139, found: 361.1151.

6-Amino-3-methyl-4-(naphthalen-1-yl)-1-phenyl-1H-pyrazolo[3,4-*b*]pyridine-5-carbonitrile (1m) Isolated as white solid, (319 mg, 85%), R_f : 0.55; Melting point: 195–197 °C; FT-IR: ν (cm^{-1}) = 3385, 3319, 2210, 1621, 776; ^1H NMR (300 MHz) δ 8.19–8.11 (m, 2H), 8.07–7.95 (m, 2H), 7.64 (dd, $J = 8.2$, 7.1, 1H), 7.59–7.43 (m, 26H), 7.36–7.28 (m, 1H), 5.47 (br. s, 2H), 1.59 (s, 3H). ^{13}C NMR (101 MHz) δ 158.5, 151.5, 150.7, 144.7, 138.8, 133.4, 131.6, 131.0, 130.2, 129.0, 128.6, 127.3, 126.6 (2C), 126.2, 125.2, 124.8, 121.5, 116.5, 110.8, 89.7, 13.4; HRMS calcd. for $\text{C}_{24}\text{H}_{17}\text{N}_5$ [M^+] 375.1484, found: 375.1503.

6-Amino-3-methyl-4-(naphthalen-2-yl)-1-phenyl-1H-pyrazolo[3,4-*b*]pyridine-5-carbonitrile (1n) Isolated as white solid, (338 mg, 90%), R_f : 0.58; Melting point: 270–272 °C; FT-IR: ν (cm^{-1}) = 3356, 3219, 2217, 1623, 744; ^1H NMR (300 MHz) δ 8.19–8.06 (m, 12H), 8.03 (d, $J = 8.5$, 1H), 7.99–7.92 (m, 3H), 7.66–7.47 (m, 5H), 7.35–7.27 (m, 1H), 5.45 (br. s, 2H), 2.02 (s, 3H). ^{13}C NMR (101 MHz) δ 158.4, 152.7, 150.9, 144.5, 138.8, 133.7, 132.7, 131.4, 129.0, 128.5 (2C), 128.0, 127.4,

127.0, 126.2, 125.7, 121.6, 116.9, 109.7, 88.7, 14.8; HRMS calcd. for $C_{24}H_{17}N_5$ [M^+] 375.1484, found. 375.1501.

6-Amino-4-(3,5-difluorophenyl)-3-methyl-1-phenyl-1H-pyrazolo[3,4-*b*]pyridine-5-carbonitrile (1o) Isolated as white solid, (314 mg, 87%), R_f : 0.67; Melting point: 198–200 °C; FT-IR: ν (cm^{-1}) = 3348, 3227, 2219, 1632, 744; 1H NMR (300 MHz) δ 8.17–8.06 (m, 2H), 7.57–7.48 (m, 2H), 7.37–7.30 (m, 1H), 7.12–6.97 (m, 3H), 5.47 (br. s, 2H), 2.10 (s, 3H). ^{13}C NMR (126 MHz) δ 162.89 (dd, $J = 252.0, 13.0$), 158.2, 150.8, 149.6, 143.8, 138.6, 136.9 (t, $J = 10.0$), 129.0, 126.4, 121.5, 116.1, 112.1 (dd, $J = 20.0, 7.0$), 109.1, 105.5 (t, $J = 25.0$), 88.1, 14.5; ^{19}F NMR (376 MHz) δ -107.5; HRMS calcd. for $C_{20}H_{13}F_2N_5$ [M^+] 361.1139, found: 361.1150.

6-Amino-4-(3,4-difluorophenyl)-3-methyl-1-phenyl-1H-pyrazolo[3,4-*b*]pyridine-5-carbonitrile (1p) Isolated as white solid, (322 mg, 89%), R_f : 0.57; Melting point: 203–205 °C; FT-IR: ν (cm^{-1}) = 3369, 3227, 2215, 1634, 764; 1H NMR (300 MHz) δ 8.15–8.08 (m, 2H), 7.56–7.48 (m, 2H), 7.43–7.30 (m, 3H), 7.27–7.21 (m, 1H), 5.46 (br. s, 2H), 2.10 (s, 3H). ^{13}C NMR (126 MHz) δ 158.2, 151.4 (dd, $J = 252.6, 12.2$), 150.9, 150.24 (dd, $J = 251.6, 12.8$), 150.0 (d, $J = 0.9$), 143.8, 138.6, 130.7 (dd, $J = 6.0, 4.3$), 129.0, 126.3, 125.2 (dd, $J = 6.6, 4.0$), 121.5, 118.1 (dd, $J = 25.0, 18.0$), 116.3, 109.3, 88.4, 14.7; ^{19}F NMR (376 MHz) δ -135.15 (dd, $J = 311.5, 21.3$); HRMS calcd. for $C_{20}H_{13}F_2N_5$ [M^+] 361.1139, found: 361.1152.

6-Amino-4-(4-cyanophenyl)-3-methyl-1-phenyl-1H-pyrazolo[3,4-*b*]pyridine-5-carbonitrile (1q) Isolated as white solid, (326 mg, 93%), R_f : 0.50; Melting point: 237–239 °C; FT-IR: ν (cm^{-1}) = 3338, 3216, 2228, 2211, 1619; 1H NMR (300 MHz) δ 8.13–8.06 (m, 2), 7.93–7.85 (m, 2H), 7.65–7.58 (m, 2H), 7.55–7.47 (m, 2H), 7.36–7.29 (m, 1H), 5.47 (br. s, 2H), 2.02 (s, 3H). ^{13}C NMR (126 MHz) δ 158.2, 150.9, 150.0, 143.6, 138.6, 132.5, 129.5, 129.0, 126.4, 121.5, 117.9, 116.2, 114.1, 109.0, 88.0, 14.7; HRMS calcd. for $C_{21}H_{14}N_6$ [M^+] 350.1280, found: 350.1303.

6-Amino-3-methyl-4-phenyl-1H-pyrazolo[3,4-*b*]pyridine-5-carbonitrile (1r) Isolated as white solid, (219 mg, 88%), Melting point: 267–269 °C; FT-IR: ν (cm^{-1}) = 3460, 3423, 3347, 3199, 2211, 1652; 1H NMR (400 MHz) δ 12.94 (s, 1H), 7.71–7.60 (m, 3H), 7.56 (dd, $J = 6.4, 2.9$ Hz, 2H), 6.98 (s, 2H), 1.87 (s, 3H). ^{13}C NMR (101 MHz, DMSO) δ 158.89, 153.19, 151.95, 142.13, 134.50, 129.38, 128.52, 128.31, 127.40, 116.97, 106.08, 86.74, 14.23.

6-Amino-3-methyl-4-(*p*-tolyl)-1H-pyrazolo[3,4-*b*]pyridine-5-carbonitrile (1s) Isolated as white solid, (226 mg, 86%), Melting point: 263–265 °C; FT-IR: ν (cm^{-1}) = 3463, 3440, 3314, 2212, 1639; 1H NMR (400 MHz) δ 12.83 (s, 1H), 7.38 (s, 4H), 6.88 (s, 2H), 2.42 (s, 3H), 1.84 (s, 3H). ^{13}C NMR (101 MHz, DMSO) δ 158.90, 153.17, 152.16, 147.12, 142.16, 138.95, 131.56, 128.85, 128.50, 117.06, 106.12, 86.82, 20.91, 14.37.

6-Amino-4-(3,4-dimethoxyphenyl)-3-methyl-1H-pyrazolo[3,4-*b*]pyridine-5-carbonitrile (1t) Isolated as white solid, (275 mg, 89%), Melting point: 273–275 °C; FT-

IR: ν (cm^{-1}) = 3413, 3325, 2924, 2213, 1652; ^1H NMR (400 MHz) δ 12.94 (s, 1H), 7.21 (d, J = 8.3 Hz, 1H), 7.19 (d, J = 1.9 Hz, 1H), 7.12 (dd, J = 8.2, 1.9 Hz, 1H), 6.92 (s, 2H), 3.94 (s, 3H), 3.88 (s, 3H), 1.99 (s, 3H). ^{13}C NMR (101 MHz, DMSO) δ 158.94, 153.25, 151.97, 149.52, 148.15, 142.23, 126.62, 121.34, 117.28, 112.40, 111.21, 106.23, 86.92, 55.65, 55.46, 14.59.

Results and discussion

Characterization of the novel nanomagnetic catalyst

To confirm the successful synthesis of the nanomagnetic heterogeneous catalyst, the structure was fully characterized by various techniques such as Fourier transform infrared spectroscopy (FT-IR), elements mapping survey with energy-dispersive X-ray spectroscopy (EDX), thermal gravimetric analysis (TGA), derivative thermal gravimetric (DTG), powder x-ray diffraction patterns (XRD), field scanning electron microscopy (FESEM), high resolution transmission electron microscopy (HRTEM), physical adsorption and physisorption of N_2 isotherms (BET) and vibrating sample magnetometer (VSM).

The FT-IR spectrum of the catalyst and its comparison with the starting materials is presented in Fig. 3. As shown, the absorption peak observed at 586 cm^{-1} is related to the formation of magnetic nanoparticles, which is attributed to the Fe–O bonds. The depicted sharp and broad band at 1076 is related to Si–O–Si stretching in the silica layer. The absorption bands at 1384 and 1629 cm^{-1} are connected to the vibrational modes of the $-\text{NO}_2$ bonds (Fig. 3).

Next, the energy-dispersive X-ray spectroscopy (EDX) and elemental mapping analyses were used to prove the organic content as well as the elemental composition of the MNPs, which could be explained by the DABCO ionic liquid tags attached to the MNPs (Figs. 4a–h). As shown, the results confirmed the presence of carbon (C: 23.73%), nitrogen (N: 12.70%), oxygen (O: 48.33%),

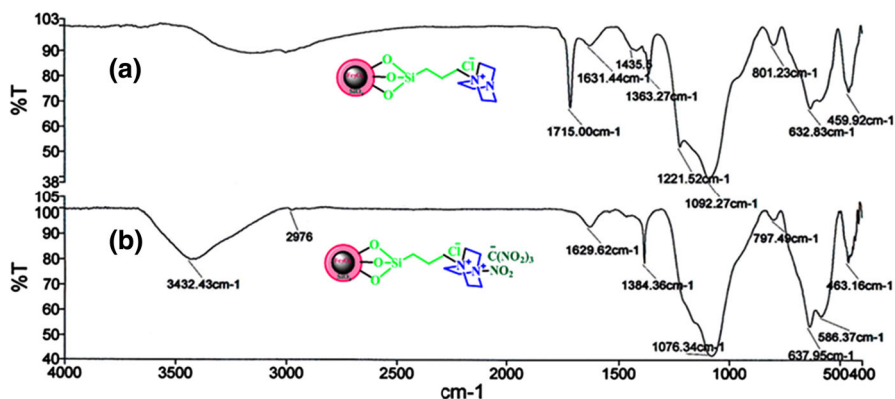


Fig. 3 FT-IR spectra of a $\text{Fe}_2\text{O}_3@SiO_2(\text{CH}_2)_3\text{-Cl}[\text{DABCO}]$, and b $\text{Fe}_2\text{O}_3@SiO_2(\text{CH}_2)_3\text{-Cl}[\text{DABCO-NO}_2]\text{C}(\text{NO}_2)_3$

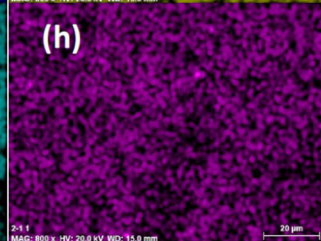
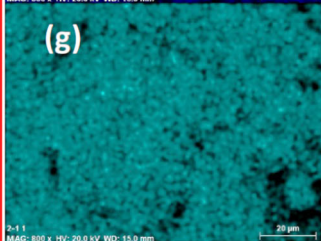
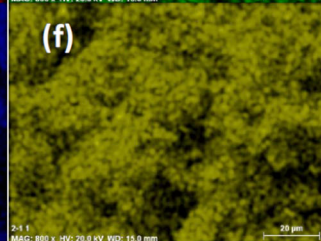
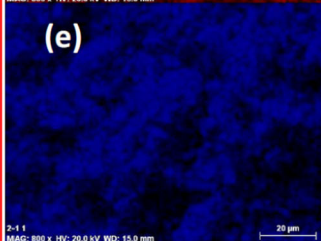
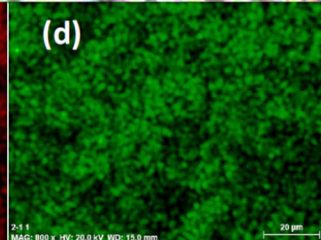
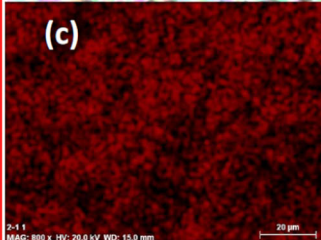
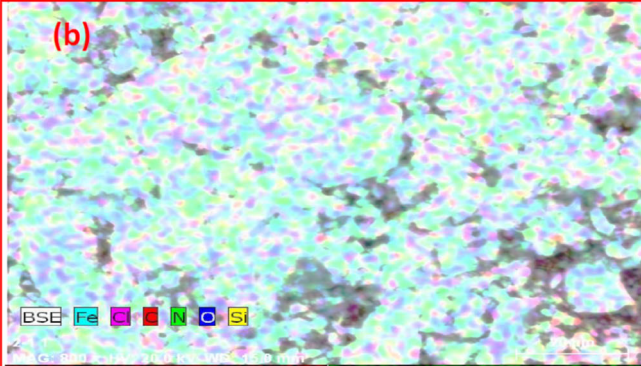
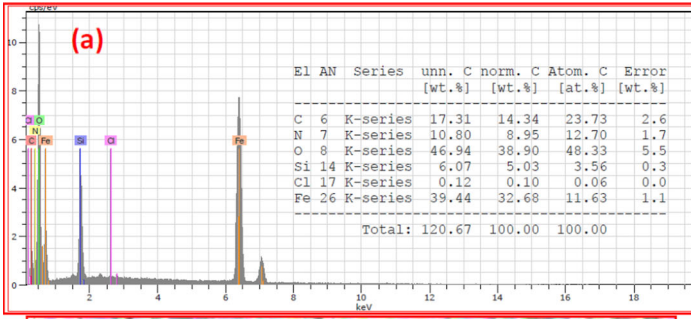
chlorine (Cl: 0.06%), iron (Fe: 11.63%) and silicon (Si: 3.56%), as the expected elements in the catalyst structure. Moreover, the selected-area elemental analysis displays the regular uniformity of the synthesized MNPs.

To investigate the morphology and topography and to resolve the internal structure of the catalyst, high-resolution transmission electron microscopy (HRTEM) and field emission scanning electron microscopy (FESEM) analyses were carried out (Fig. 5). As shown in figures a and b, Fe_2O_3 has been coated with tetraethyl orthosilicate (TEOS), 3-chloropropyltrimethoxysilane, 1,4-diazabicyclo[2.2.2]octane (DABCO) and tetranitromethane respectively. The shape of $\text{Fe}_2\text{O}_3@ \text{SiO}_2(\text{CH}_2)_3\text{-Cl}[\text{DABCO-NO}_2]\text{C}(\text{NO}_2)_3$ were separated, arranged and improved to a symmetrical double spherical MNPs. As shown in Fig. 5b, the crystal Fe_2O_3 -MNPs distance layer of final nanoparticles is around 0.26 nm. Moreover, the FESEM results clearly proved the spherical and uniform shape of the MNPs in the sample (Fig. 5c).

Thermogravimetric (TG) analysis, derivatives thermal gravimetric analysis (DTG), and the differential thermal analysis (DSC) were performed to analyze the content of DABCO ionic tags in the catalyst under argon atmosphere (Fig. 6). From the performed studies, it can be inferred that of the two main weight losses that occurred upon heating, the first, from ambient temperature to 110 °C with a weight loss of ~ 1 wt% could be related to the removal of surface-adsorbed water and organic solvents applied during the catalyst preparation, and the second part from 200 to 300 °C with weight loss of > 11 wt% could be reason for the ionic molten salt nature of DABCO with different NO_2 parts. Moreover, the analysis of the results of DSC (Fig. 6b) showed that the catalyst has three different thermal behaviours. Initially, it showed a downward and exothermic pattern from 25 to 110 °C. Then, a second upwards and endothermic pattern from 110 to ~ 400 °C, and finally, in the last part from ~ 400 to 800 °C it showed again a downward and endothermic behaviour.

Further observations were obtained by powder X-ray diffraction (XRD) to illustrate the crystalline structure of the MNPs in a range of $10 < 2\theta < 90^\circ$ (Fig. 7). The upward typical iron oxide spectrum pattern showed peaks at 2θ values of 14.96° , 18.38° , 30.24° , 35.63° , 43.28° , 53.73° , 57.27° , 62.93° and 74.47° related to (110), (111), (220) (311), (400), (422), (511), (440) and (533) corresponding to planes of iron oxide (Fe_xO_y). Moreover, as is clear from the maghemite (Fe_2O_3) with blue standard lines (JCP2: 00-039-1346) and magnetite (Fe_3O_4) with red standard lines (JCP2: 01-075-1609) as the standard references, the center of every peak may be adjusted with maghemite (Fe_2O_3) structures more than magnetite (Fe_3O_4). Also, the sharpest peak in the XRD spectrum of the catalyst has been correlated to plane (311) at 30.24° with a 2.51 Å layer distance, and the largest layer distance is correlated to layer (220) at 30.24° with 2.95 Å.

Next, N_2 adsorption/desorption isotherm was performed to characterize the porosity and total surface area of the magnetic nanoparticles. As shown in Fig. 8a, catalyst exhibited type II isotherm according to the IUPAC definition and with H_3 type hysteresis loop, which displayed the presence of a nanoporous structure. The surface area and pore volume of the catalyst are listed in Table 1. The obtained Brunauer–Emmett–Teller (BET), BJH and DR specific surface areas of



◀ **Fig. 4** **a** EDX spectroscopy quantitative analysis; **b** total elemental maps and displays of C (**c**), N (**d**), O (**e**), Si (**f**), Fe (**g**), and Cl (**h**) atoms in the MNPs of catalyst

$\text{Fe}_2\text{O}_3@\text{SiO}_2(\text{CH}_2)_3\text{-Cl}[\text{DABCO-NO}_2]\text{C}(\text{NO}_2)_3$ are 112.766, 61.676 and 108.923 $\text{m}^2 \text{g}^{-1}$, respectively. Moreover, the total pore volume was determined to be 0.31 $\text{cm}^3 \text{g}^{-1}$. The corresponding pore-size distribution (PSD) of nanopores (inset of Figs. 8b) was calculated from the adsorption branch on the basis of BJH model (Fig. 8b) and is centered at 15 nm, according to the (BJH) model.

The magnetic measurement of $\text{Fe}_2\text{O}_3@\text{SiO}_2(\text{CH}_2)_3\text{-Cl}[\text{DABCO-NO}_2]\text{C}(\text{NO}_2)_3$ was also studied. Its VSM was compared with its precursors Fe_2O_3 , $\text{Fe}_2\text{O}_3@\text{SiO}_2$ and $\text{Fe}_2\text{O}_3@\text{SiO}_2(\text{CH}_2)_3\text{Cl}$. As shown in Fig. 9, after the addition of each layer, the saturation magnetization reduced from 70.55 emu g^{-1} for Fe_2O_3 to 50.01 emu g^{-1} for the described $\text{Fe}_2\text{O}_3@\text{SiO}_2(\text{CH}_2)_3\text{-Cl}[\text{DABCO-NO}_2]\text{C}(\text{NO}_2)_3$.

After the full characterization and investigation of the catalyst's structure, it was used as nanomagnetic catalyst in the condensation reaction of 3-methyl-1-phenyl-1*H*-pyrazol-5-amine or 3-methyl-1*H*-pyrazol-5-amine, malononitrile and various aromatic aldehydes for the synthesis of pyrazolo[3,4-*b*]pyridine derivatives. Initially, the reaction of benzaldehyde, 3-methyl-1-phenyl-1*H*-pyrazol-5-amine and malononitrile was selected as a model by which to optimize the reaction conditions. The results for the optimization of temperature, catalyst loading and solvents are summarized in Table 2. As shown, the best results for the synthesis of pyrazolo[3,4-*b*]pyridines were achieved when the reaction was carried out at 100 °C in the presence of 5 mg of $\text{Fe}_2\text{O}_3@\text{SiO}_2(\text{CH}_2)_3\text{-Cl}[\text{DABCO-NO}_2]\text{C}(\text{NO}_2)_3$ under neat conditions.

After optimizing the reaction conditions, to assess the scope and limitations of the catalyst, 3-methyl-1-phenyl-1*H*-pyrazol-5-amine or 3-methyl-1*H*-pyrazol-5-amine was reacted with various aromatic aldehydes (bearing electron-donating and electron-withdrawing groups) and malononitrile. As shown in Table 3, the results indicated that this method is appropriate for the synthesis of pyrazolo[3,4-*b*]pyridine derivatives, regardless of the structure of the aromatic aldehyde employed in the reaction. Aliphatic aldehyde was also tested; the target products were not synthesized. The reaction was sluggish.

In accord with previously reported methods [28, 31], an applicable mechanism for the synthesis of pyrazolo[3,4-*b*]pyridines is proposed (Scheme 2). Firstly, malononitrile reacts with the catalyst-activated aldehyde to afford 2-benzylidene-malononitrile (**II**), after losing nitric acid [36]. Then, 3-methyl-1-phenyl-1*H*-pyrazol-5-amine or 3-methyl-1*H*-pyrazol-5-amine attacks to intermediate **II** as a Michael acceptor to afford **III**. Next, the intramolecular cyclization of **III** creates intermediate **IV** which is converted to the desired product via hyperconjugative-like anomeric-based oxidation (Scheme 3). Previously reported studies have proposed an aerobic oxidation of intermediate **V** towards the target molecule **VII**. In contrast to the previously reported mechanistic route [31] for the final step of the aforementioned described organic mechanism, we suggest that this step might proceed via an unusual hydride transfer/Cannizzaro reaction (Scheme 4) [37] such as those proposed for pyranose acetals (Scheme 5) [38] and the H_2 releasing from

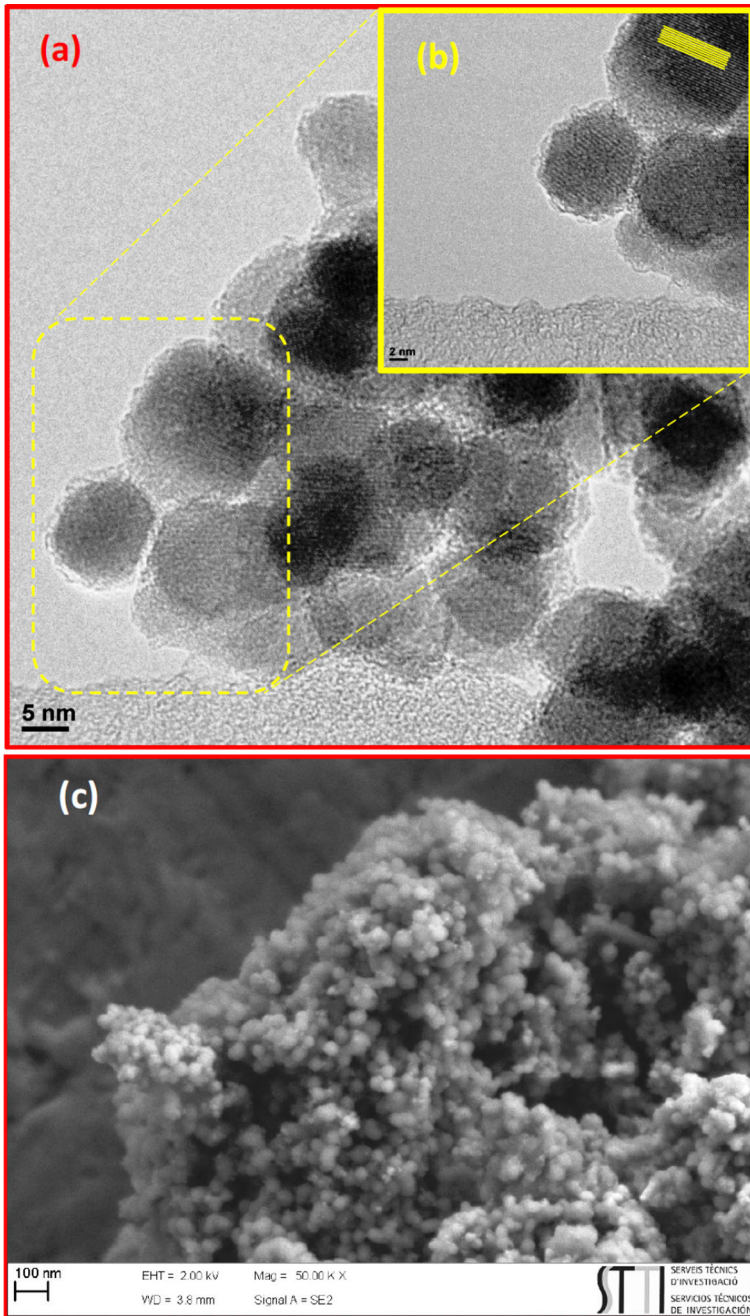


Fig. 5 a) High resolution transmission electron microscopy (HRTEM) images of a) $\text{Fe}_2\text{O}_3@ \text{SiO}_2(\text{CH}_2)_3\text{-Cl}[\text{DABCO-NO}_2]\text{C}(\text{NO}_2)_3$ in 5 nm scale; inset: b) 2 nm selected scale area (V); and c) field emission scanning electron microscopy (FESEM) of final catalyst nanoparticles in 100 nm scale

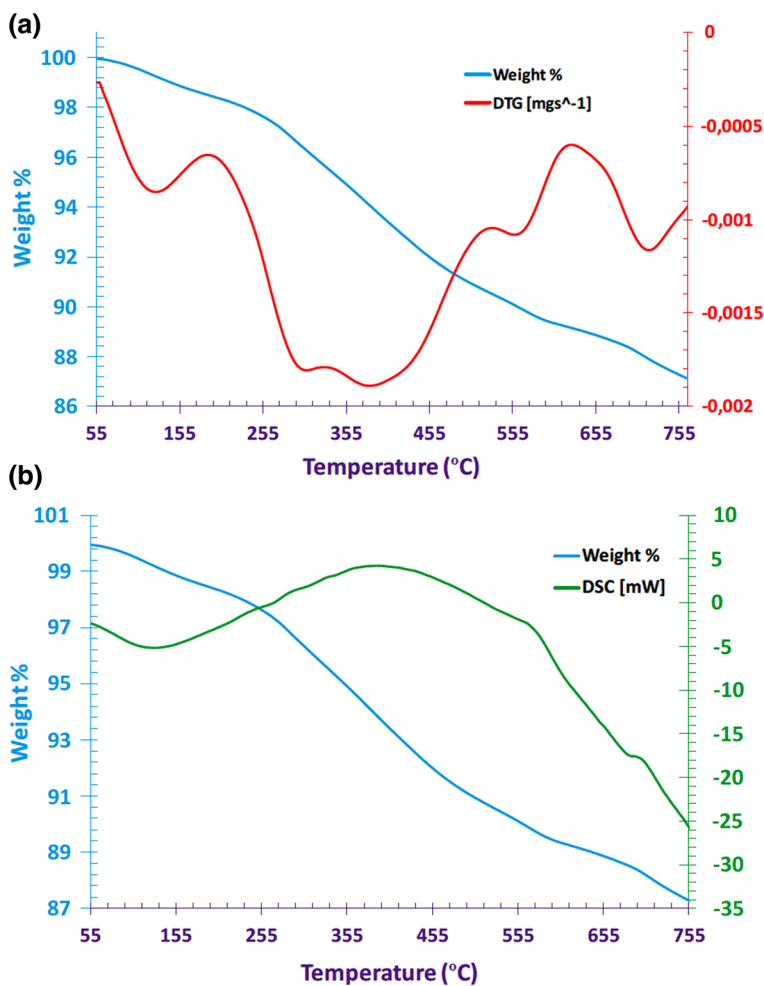


Fig. 6 **a** Thermal gravimetric analysis (TG/DTG), and **b** (TGA/DSC) of MNPs

tricyclic orthoamides (Scheme 6) [39–41]. As presented in Scheme 7, the isomer with an equatorial methoxy group is more reactive than its axial counterpart due to the presence of two lone pair anomeric assistance, which facilitates the departure of the hydride leaving group [38].

As mentioned above, we have introduced an “anomeric-based oxidation (ABO)” terminology for the final step towards the synthesis of various molecules such as: 1,4-dihydropyrano-[2,3-*c*]pyrazoles [42, 43], 2,4,6-triarylpyridines [44, 45], 2-amino-3-cyanopyridines [46, 47], 2-substituted benz-(imida, oxa and othia)-zole derivatives [36], the oxidative aromatization of pyrazolines and 1,4-dihydropyridines [48], sulfanylpyridines [49], and 2-amino-4-aryl-6-(arylamino)pyridine-3,5-dicarbonitriles [50]. To validate this idea, the model reaction was carried out under

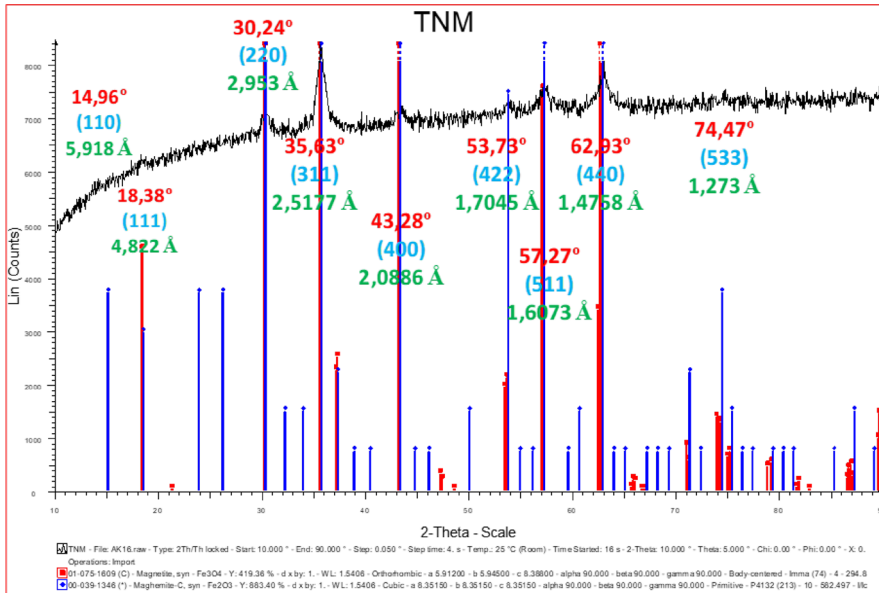


Fig. 7 Powder XRD pattern of MNPs, inlet blue solid lines: JCP2: 00-039-1346 for standard data base of Fe_2O_3 and inlet red solid lines: (JCP2: 01-075-1609) for standard data base of Fe_3O_4

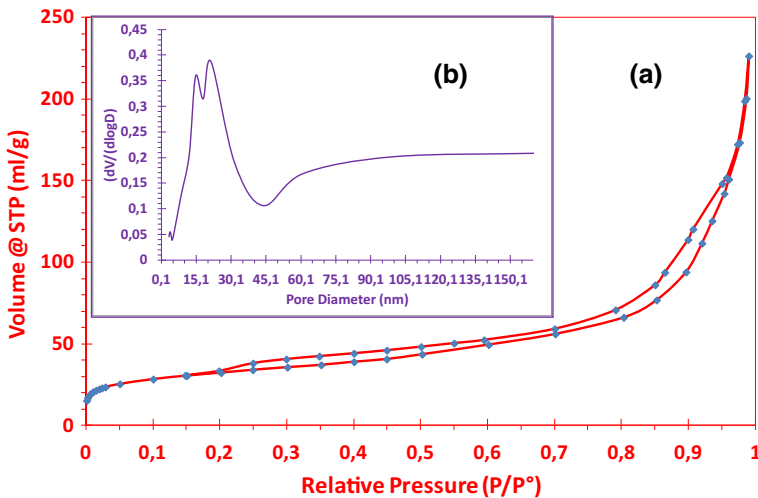
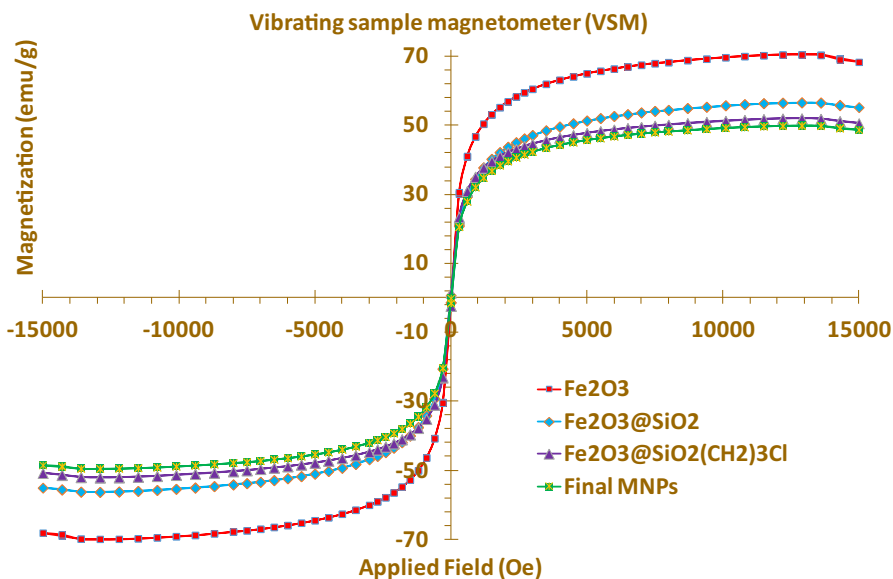


Fig. 8 a Nitrogen adsorption/desorption isotherms and **b** inset: BJH pore size distribution of $\text{Fe}_2\text{O}_3@ \text{SiO}_2(\text{CH}_2)_3\text{-Cl}[\text{DABCO-NO}_2]\text{C}(\text{NO}_2)_3$

both nitrogen and argon atmosphere in the absence of any molecular oxygen. Under these conditions, the reaction progressed under atmosphere of nitrogen and argon slightly slower than under normal reaction conditions (air atmosphere). On the basis

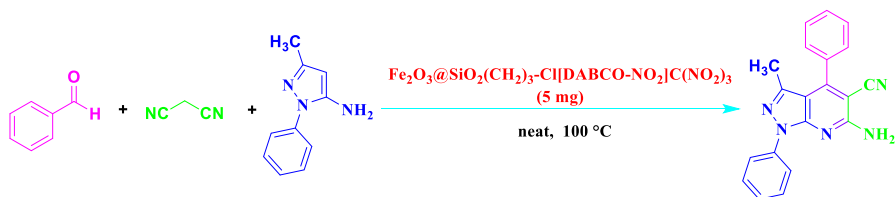
Table 1 Textural properties of $\text{Fe}_2\text{O}_3@\text{SiO}_2(\text{CH}_2)_3\text{-Cl}[\text{DABCO-NO}_2]\text{C}(\text{NO}_2)_3$

$S_{\text{BET}}^{\text{a}}$ ($\text{m}^2 \text{g}^{-1}$)	$S_{\text{BJH}}^{\text{b}}$ ($\text{m}^2 \text{g}^{-1}$)	S_{m}^{c} ($\text{m}^2 \text{g}^{-1}$)	V_{t}^{d} ($\text{cm}^3 \text{g}^{-1}$)	Pore size ^e (nm)
112.766	61.676	108.923	0.31	14.826

^a S_{BET} : total surface area^b S_{BJH} : surface area estimated by BJH model applied to the desorption branch of the isotherm^c S_{m} : Micropore surface area estimated by DR model^d V_{t} : total pore volume^eObtained from BJH**Fig. 9** VSM magnetization curves of catalyst compared to the catalyst precursors Fe_2O_3 , $\text{Fe}_2\text{O}_3@\text{SiO}_2$, $\text{Fe}_2\text{O}_3@\text{SiO}_2(\text{CH}_2)_3\text{Cl}$

of this evidence, the conversion of intermediate **V** to the target molecule **VII** might occur by unusual hydride transfer and the release of molecular hydrogen (H_2). The C–H bond is weakened via hyperconjugation, like that of the nitrogen lone pairs into the anti-bonding of C–H ($\sigma_{\text{C-H}}^*$ orbital) which can be broken by reaction with a proton to give molecular hydrogen.

The recovery and reuse of $\text{Fe}_2\text{O}_3@\text{SiO}_2(\text{CH}_2)_3\text{-Cl}[\text{DABCO-NO}_2]\text{C}(\text{NO}_2)_3$ were investigated under the optimized conditions for the reaction of benzaldehyde, 3-methyl-1-phenyl-1*H*-pyrazol-5-amine and malononitrile. In these conditions, the nanomagnetic catalyst was reused up to nine times with only a marginal decrease in its reactivity. After each use, in order to recover the catalyst, acetone was added to

Table 2 Reaction of benzaldehyde, 3-methyl-1-phenyl-1*H*-pyrazol-5-amine and malononitrile under different conditions

Entry	Solvent	Catalyst loading (mg)	Temp. (°C)	Time (min)	Yield (%) ^a
1	–	10	80	30	81
2	–	10	100	25	89
3	–	10	100	25	89
4	–	8	100	25	89
5	–	5	100	25	89
6	–	3	100	40	75
7	–	–	100	180	38
8	EtOH	5	Reflux	240	35
9	EtOAc	5	Reflux	180	32
10	H ₂ O	5	Reflux	240	Trace
11	CH ₃ CN	5	Reflux	180	38

Reaction conditions: aryl aldehyde (1 mmol), malononitrile (1.2 mmol, 79 mg), 3-methyl-1-phenyl-1*H*-pyrazol-5-amine (1 mmol, 173 mg) and [Fe₂O₃@SiO₂(CH₂)₃-Cl[DABCO-NO₂]C(NO₂)₃] (5 mg)

Bold value indicates the optimized conditions

^aIsolated yield

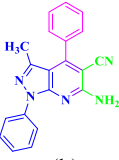
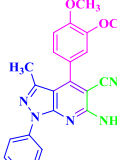

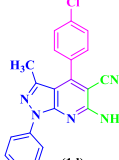

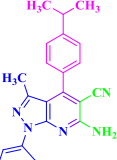

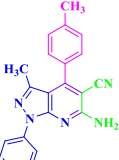
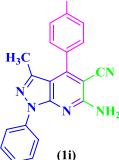
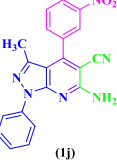





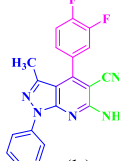


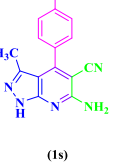

the reaction mixture. Then, the catalyst was recovered by using an external magnet and reused in the subsequent reactions after washing with acetone. As shown in Fig. 10, the activity of the catalyst was maintained up to nine times without any significant changes in the yields and reaction times.

Efficiency and applicability of [Fe₂O₃@SiO₂(CH₂)₃-Cl[DABCO-NO₂]C(NO₂)₃] for the synthesis of pyrazolo[3,4-*b*]pyridines compared with some other reported nanomagnetic catalysts. As shown in Table 4, [Fe₂O₃@SiO₂(CH₂)₃-Cl[DABCO-NO₂]C(NO₂)₃] is better than those previously reported catalysts in yields and reaction times for the reactions of benzaldehyde, 3-methyl-1-phenyl-1*H*-pyrazol-5-amine and malononitrile.

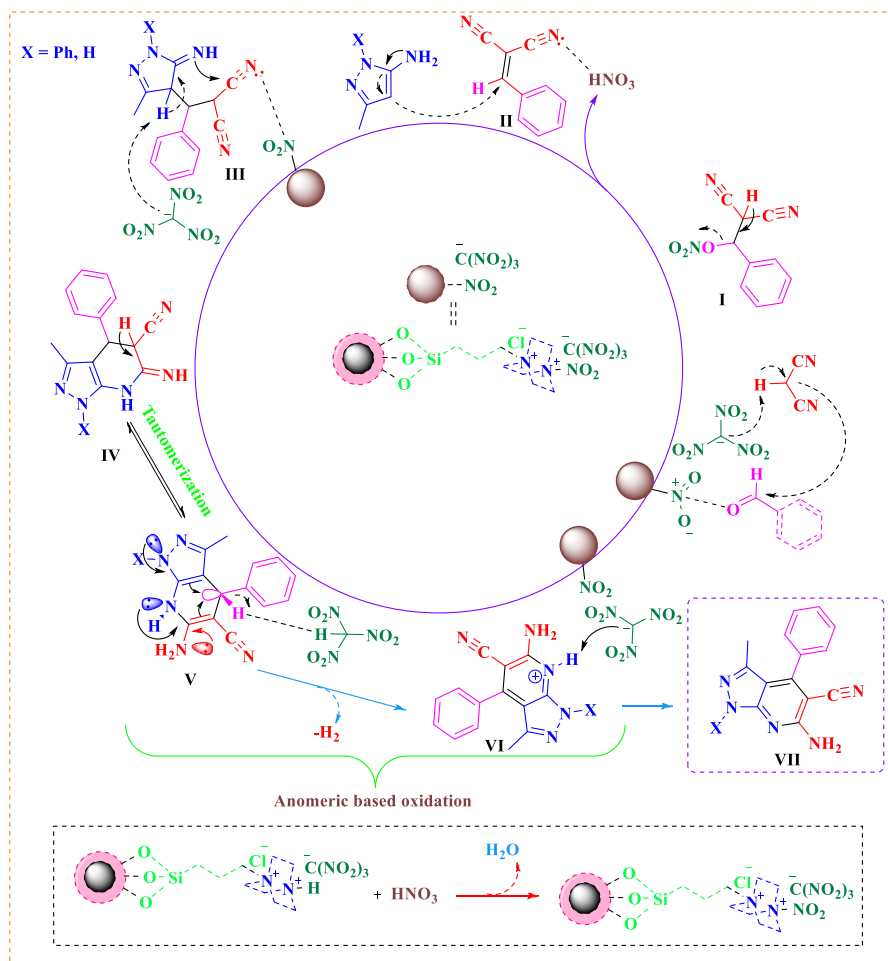
Conclusion

In summary, as a continuation of our studies with new nanomagnetic catalysts [51–56], the magnetic nanoparticles (MNPs) surface was chemically modified with Cl[DABCO-NO₂]C(NO₂)₃ tags and the obtained Fe₂O₃@SiO₂(CH₂)₃-Cl[DABCO-NO₂]C(NO₂)₃ was fully characterized by several techniques such as, FT-IR, EDX/

Table 3 Synthesis of pyrazolo[3,4-*b*]pyridine derivatives using $\text{Fe}_2\text{O}_3@\text{SiO}_2(\text{CH}_2)_3\text{-Cl}[\text{DABCO-NO}_2]\text{-C}(\text{NO}_2)_3$ as a new nanomagnetic catalyst under neat conditions

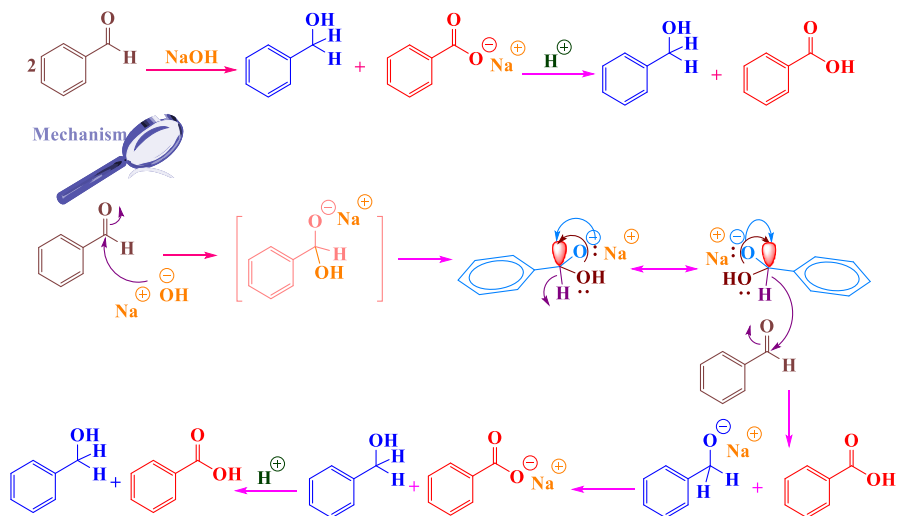
 (1a) time: 25 min; yield: 89%; Mp: 210-212 °C ³¹	 (1b) time: 35 min; yield: 92%; Mp: 218-220 °C ²⁸	 (1c) time: 20 min; yield: 90%; Mp: 223-225 °C ³¹	 (1d) time: 20 min; yield: 91%; Mp: 194-198 °C ²⁸
 (1e) time: 25 min; yield: 92%; Mp: 216-217 °C ³¹	 (1f) time: 35 min; yield: 87%; Mp: 198-200 °C	 (1g) time: 30 min; yield: 91%; Mp: 167-169 °C	 (1h) time: 30 min; yield: 93%; Mp: 200-202 °C ²⁸
 (1i) time: 20 min; yield: 88%; Mp: 214-216 °C ²⁸	 (1j) time: 20 min; yield: 85%; Mp: 157-159 °C ³¹	 (1k) time: 25 min; yield: 91%; Mp: 195-197 °C ²⁸	 (1l) time: 35 min; yield: 85%; Mp: 227-229 °C
 (1m) time: 35 min; yield: 85%; Mp: 195-197 °C	 (1n) time: 30 min; yield: 90%; Mp: 270-272 °C	 (1o) time: 25 min; yield: 87%; Mp: 198-200 °C	 (1p) time: 25 min; yield: 89%; Mp: 203-205 °C
 (1q) time: 25 min; yield: 93%; Mp: 237-239 °C	 (1r) time: 30 min; yield: 88%; Mp: 267-269 °C	 (1s) time: 35 min; yield: 86%; Mp: 263-265 °C	 (1t) time: 35 min; yield: 89%; Mp: 273-275 °C

Reaction conditions: aryl aldehyde (1 mmol), malononitrile (1.2 mmol, 79 mg), 3-methyl-1-phenyl-1H-pyrazolo-5-amine or 3-methyl-1H-pyrazolo-5-amine (1 mmol) and $[\text{Fe}_2\text{O}_3@\text{SiO}_2(\text{CH}_2)_3\text{-Cl}[\text{DABCO-NO}_2]\text{-C}(\text{NO}_2)_3]$ (5 mg)

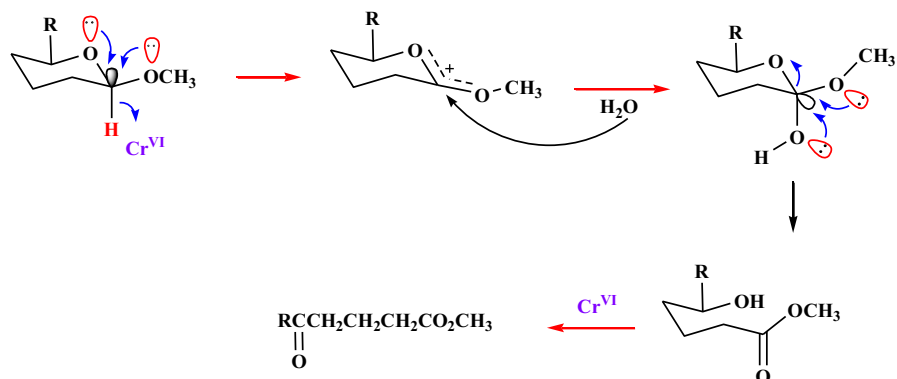


Scheme 3 The proposed mechanism for the synthesis of pyrazolo[3,4-*b*]-pyridines in the presence of $\text{Fe}_2\text{O}_3@(\text{SiO}_2(\text{CH}_2)_3\text{-Cl[DABCO-NO}_2\text{]C(NO}_2)_3)$

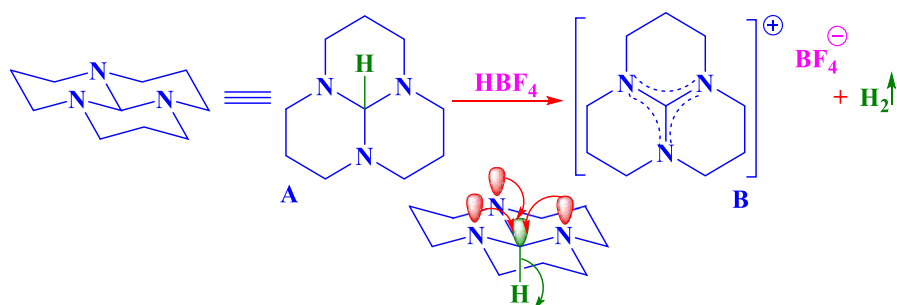
mapping, FESEM, HRTEM, TGA, DTG, DSC, powder XRD, N_2 adsorption (BET) and VSM. The described nanomagnetic particles were used as an efficient catalyst for the three-component condensation reaction of aryl aldehydes, 3-methyl-1-phenyl-1*H*-pyrazol-5-amine or 3-methyl-1*H*-pyrazol-5-amine and malononitrile under neat conditions. Short reaction times, good yields, easy work-up and reusability of catalyst are also major advantages of this methodology. Finally, an anomer-based oxidation was suggested for the final step of the pyrazolo[3,4-*b*]pyridines synthesis.



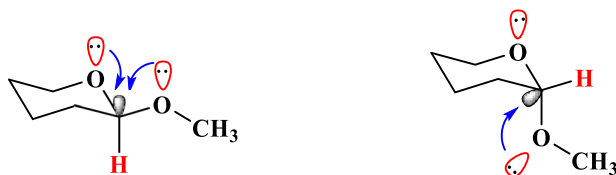
Scheme 4 Suggested mechanism for the in situ oxidation–reduction Cannizzaro reaction by an uncommon hydride transfer via ABO mechanism [37]



Scheme 5 Unusual hydride transfer from 2-methoxypropanoate by ABO mechanism [38]



Scheme 6 Unusual hydride transfer from tricyclic orthoamide (A) by ABO mechanism [39–41]



Two lone pair orbitals in antiperiplanar arrangement

Only one lone pair orbital in antiperiplanar arrangement

Scheme 7 Isomer with equatorial 2-methoxy group is more reactive than its axial isomer due to the presence of two lone pair anomeric assistance to the departure of the hydride leaving group [38]

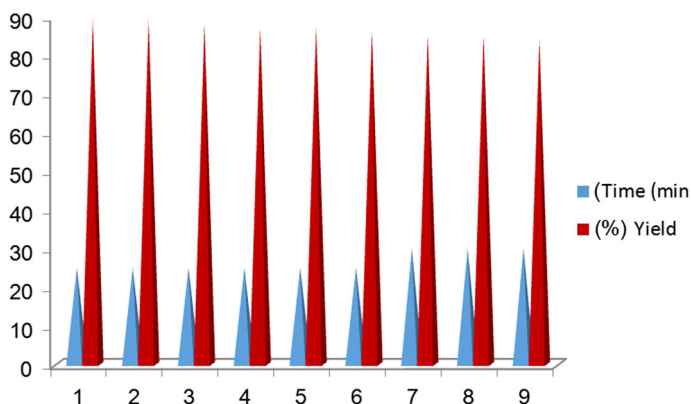


Fig. 10 Reactions of benzaldehyde, 3-methyl-1-phenyl-1*H*-pyrazol-5-amine and malononitrile using the recycled catalyst

Table 4 Evaluation of various catalyst for the synthesis of pyrazolo[3,4-*b*]pyridines in solvent free conditions

Entry	Catalyst	Catalyst loading	Time (min)	Yield (%)	Refs.
1	[Fe ₂ O ₃ @SiO ₂ (CH ₂) ₃ -Cl][DABCO-NO ₂]C(NO ₂) ₃]	5 mg	25	89	^a
2	[Fe ₃ O ₄ @SiO ₂ (CH ₂) ₃ -DABCO-SO ₃ H]Cl ₂	5 mg	30	86	[57]
3	[Fe ₃ O ₄ @SiO ₂ (CH ₂) ₃ S-SO ₃ H]	5 mg	30	84	[58]
4	[Fe ₃ O ₄ @SiO ₂ (CH ₂) ₃ -Im-SO ₃ H]Cl	5 mg	30	85	[59]
5	[Fe ₃ O ₄ @SiO ₂ (CH ₂) ₃ NH ₂]	5 mg	60	45	[60]

^aThis work

Acknowledgements We thank Bu-Ali Sina University, Iran National Science Foundation (INSF) (Grant Number: 95831207), National Elites Foundation, University of Alicante (VIGROB-173, UAUSTI16-03), and the Spanish Ministerio de Economía y Competitividad (CTQ2015-66624-P) for financial support to our research groups.

References

1. O. Deuschmann, H. Knözinger, K. Kochloefl, T. Turek, *Heterogeneous Catalysis and Solid Catalysts* (Wiley, Weinheim, 2009)
2. M.A. Zolfigol, T. Azadbakht, V. Khakyzadeh, R. Nejatyami, D. Perrin, *RSC Adv.* **4**, 40036 (2014)
3. M.A. Zolfigol, V. Khakyzadeh, A.R. Moosavi-Zare, A. Rostami, A. Zare, N. Iranpoor, M.H. Beyzavi, R. Luque, *Green Chem.* **15**, 2132 (2013)
4. H. Sharghi, A. Khoshnood, M.M. Doroodmand, R. Khalifeh, *J. Iran. Chem. Soc.* **9**, 231 (2012)
5. H. Sharghi, A. Khoshnood, R. Khalifeh, M.M. Doroodmand, *Mol. Divers.* **19**, 481 (2015)
6. S.B. Sapkal, K.F. Shelke, B.B. Shingate, M.S. Shingare, *Tetrahedron Lett.* **50**, 1754 (2009)
7. M. Fallah-Mehrjardi, *Mini. Rev. Org. Chem.* **14**, 122 (2017)
8. M. Mokhtary, *J. Iran. Chem. Soc.* **13**, 1827 (2016)
9. V. Polshettiwar, R. Luque, A. Fihri, H. Zhu, M. Bouhrara, J.M. Basset, *Chem. Rev.* **111**, 3036 (2011)
10. B. Karimi, F. Mansouri, H.M. Mirzaei, *ChemCatChem* **7**, 1736 (2015)
11. D. Zhang, C. Zhou, Z. Sun, L.Z. Wu, C.H. Tung, T. Zhang, *Nanoscale* **4**, 6244 (2012)
12. M.B. Gawande, P.S. Branco, R.S. Varma, *Chem. Soc. Rev.* **42**, 3371 (2013)
13. S. Hu, Y. Guan, Y. Wang, H. Han, *Appl. Energ.* **88**, 2685 (2011)
14. A. Khazaei, M.A. Zolfigol, A.R. Moosavi-Zare, J. Afsar, A. Zare, V. Khakyzadeh, M.H. Beyzavi, *Chin. J. Catal.* **34**, 1936 (2013)
15. M.A. Zolfigol, M. Yarie, *RSC Adv.* **5**, 103617 (2015)
16. H. Sharghi, A. Khoshnood, M.M. Doroodmand, R. Khalifeh, *J. Heterocycl. Chem.* **53**, 164 (2016)
17. E. Juaristi, G. Cuevas, *Tetrahedron* **48**, 5019 (1992)
18. S.A. Glover, *Tetrahedron* **54**, 7229 (1998)
19. E. Juaristi, Y. Bandala, *Adv. Heterocycl. Chem.* **105**, 189 (2012)
20. C.M. Filloux, *Angew. Chem. Int. Ed.* **54**, 8880 (2015)
21. M. Yarie, *Iran. J. Catal.* **7**, 85 (2017)
22. G. Hamasaka, H. Tsuji, Y. Uozumi, *Synlett* **26**, 2037 (2015)
23. T. He, R. Shi, Y. Gong, G. Jiang, M. Liu, S. Qian, Z. Wang, *Synlett* **27**, 1864 (2016)
24. C.-B. Bai, N.-X. Wang, Y. Xing, X.-W. Lan, *Synlett* **28**, 402 (2017)
25. N.-X. Wang, J. Zhao, *Synlett* **18**, 2785 (2007)
26. L.F. Pedrosa, W.P. de Macedo, A.C.R. Furtado, G.P. Guedes, J.C. Borges, J.A.L.C. Resende, M.G.F. Vaz, A.M.R. Bernardino, M.C. de Souza, *ARKIVOC* **iv**, 38 (2014)
27. V. Kumar, K. Kaur, G.K. Gupta, A.K. Sharma, *Eur. J. Med. Chem.* **69**, 735 (2013)
28. D.-Q. Shi, H. Yao, J.-W. Shi, *Synth. Commun.* **38**, 1662 (2008)
29. I.H. Eissa, A.M. El-Naggar, M.A. El-Hashash, *Bioorg. Chem.* **67**, 43 (2016)
30. T.I. El-Emary, *J. Chin. Chem. Soc.* **54**, 507 (2007)
31. X. Zhang, X. Li, X. Fan, X. Wang, J. Wang, G. Qu, *Aust. J. Chem.* **62**, 382 (2009)
32. Y.L. Chen, *Chem. Abstr.* **124**, 232447 (1995)
33. J. Quiroga, S. Cruz, B. Insuasty, R. Abonia, *J. Heterocycl. Chem.* **38**, 53 (2001)
34. B. Zhao, Y. Li, P. Xu, Y. Dai, C. Luo, Y. Sun, J. Ai, M. Geng, W. Duan, *ACS Med. Chem. Lett.* **7**, 629 (2016)
35. M.D. Hill, H. Fang, J.M. Brown, T. Molski, A. Easton, X. Han, R. Miller, M. Hill-Drzewi, L. Gallagher, M. Matchett, M. Gulianello, A. Balakrishnan, R.L. Bertekap, K.S. Santone, V.J. White-rock, X. Zhuo, J.J. Bronson, J.E. Macor, A.P. Degnan, *ACS Med. Chem. Lett.* **7**, 1082 (2016)
36. M.A. Zolfigol, A. Khazaei, S. Alaie, S. Baghery, F. Maleki, Y. Bayat, A. Asghari, *RSC Adv.* **6**, 58667 (2016)
37. M.A. Zolfigol, H. Gholami, V. Khakyzadeh, *Principles of Organic Synthesis with a New Approach*, 3rd edn. (Bu-Ali Sina University Publishers, Hamedan, 2014), p. 26
38. S.J. Angyal, K. James, *Aust. J. Chem.* **23**, 1209 (1970)
39. J.M. Erhardt, J.D. Wuest, *J. Am. Chem. Soc.* **102**, 6363 (1980)
40. T.J. Atkins, *J. Am. Chem. Soc.* **102**, 6364 (1980)
41. J.M. Erhardt, E.R. Grover, J.D. Wuest, *J. Am. Chem. Soc.* **102**, 6365 (1980)
42. M.A. Zolfigol, F. Afsharnadery, S. Baghery, S. Salehzadeh, F. Maleki, *RSC Adv.* **5**, 75555 (2015)
43. M.A. Zolfigol, M. Safaiee, F. Afsharnadery, N. Bahrani-Nejad, S. Baghery, S. Salehzadeh, F. Maleki, *RSC Adv.* **5**, 100546 (2015)
44. A.R. Moosavi-Zare, M.A. Zolfigol, Z. Rezanejad, *Can. J. Chem.* **94**, 626 (2016)
45. M.A. Zolfigol, M. Kiafar, M. Yarie, A. Taherpour, M. Saeidi-Rad, *RSC Adv.* **6**, 50100 (2016)

46. M.A. Zolfigol, M. Yarie, *Appl. Organometal. Chem.* **31**, 3598 (2017)
47. M.A. Zolfigol, M. Kiafar, M. Yarie, A. Taherpour, T. Fellowes, A.N. Hancock, A. Yari, *J. Mol. Struct.* **1137**, 674 (2017)
48. M. Kiafar, M.A. Zolfigol, M. Yarie, A. Taherpour, *RSC Adv.* **6**, 102280 (2016)
49. M.A. Zolfigol, M. Safaiee, B. Ebrahimghasri, S. Baghery, S. Alaie, M. Kiafar, A. Taherpour, Y. Bayat, A. Asgari, *J. Iran. Chem. Soc.* **14**, 1839 (2017)
50. S. Baghery, M.A. Zolfigol, F. Maleki, *New J. Chem.* **41**, 9276 (2017)
51. N. Koukabi, E. Kolvari, A. Khazaei, M.A. Zolfigol, B.S. Shaghasemi, H.R. Khavasi, *Chem. Commun.* **47**, 9230 (2011)
52. N. Koukabi, E. Kolvari, M.A. Zolfigol, A. Khazaei, B.S. Shaghasemi, B. Fasahati, *Adv. Synth. Catal.* **354**, 2001 (2012)
53. T. Azadbakht, M.A. Zolfigol, R. Azadbakht, V. Khakizadeh, D. Perrin, *New J. Chem.* **39**, 439 (2015)
54. M. Safaiee, M.A. Zolfigol, F. Afsharnadery, S. Baghery, *RSC Adv.* **5**, 102340 (2015)
55. M. Yarie, M.A. Zolfigol, Y. Bayat, A. Asgari, D.A. Alonso, A. Khoshnood, *RSC Adv.* **6**, 82842 (2016)
56. L. Mohammadi, M.A. Zolfigol, M. Ebrahimiinia, K.P. Roberts, S. Ansari, T. Azadbakht, S.R. Hus-saini, *Catal. Commun.* **102**, 44 (2017)
57. M. Rajabi-Salek, M.A. Zolfigol, M. Zarei, *Res. Chem. Intermed.* (2018)
58. S. Moradi, M.A. Zolfigol, M. Zarei, D.A. Alonso, A. Khoshnood, A. Tajally, *Appl. Organomet. Chem.* (2018).
59. M.A. Zolfigol, R. Ayazi-Nasrabadi, S. Baghery, V. Khakyzadeh, S. Azizian, *J. Mol. Catal. A Chem.* **418–419**, 54 (2016)
60. M.A. Zolfigol, A.R. Moosavi-Zare, M. Zarei, A. Zare, E. Noroozizadeh, R. Karamian, M. Asadbegy, *RSC Adv.* **6**, 62460 (2016)

Affiliations

Javad Afsar¹ · Mohammad Ali Zolfigol¹  · Ardeshir Khazaei¹ · Diego A. Alonso² · Abbas Khoshnood² · Yadollah Bayat³ · Asiye Asgari³

¹ Department of Organic Chemistry, Faculty of Chemistry, Bu-Ali Sina University, Hamedan 6517838683, Iran

² Organic Chemistry Department, Organic Synthesis Institute, Alicante University, Apdo. 99, 03080 Alicante, Spain

³ Faculty of Chemistry and Chemical Engineering, Malek Ashtar University of Technology, Tehran, Iran